Optimization of E. Coli Tip-Sonication for High-Yield Cell Free Extract using Finite Element Modeling

By Sakib Ferdous[1], Jared L. Dopp[1], and Nigel F. Reuel[1]*

1. Department of Chemical and Biological Engineering, Iowa State University

*reuel@iastate.edu

*Corresponding author: Dr Nigel F. Reuel

Address: 3051 Sweeney

618 Bissell Rd.

Ames, IA 50011-1098

Email: reuel@iastate.edu

Phone: 515-294-4592

Funding

This work was supported by NIGMS MIRA ESI Award #1R35GM138265-01

Abstract

Optimal tip sonication settings, namely tip position, input power, and pulse durations, are necessary for temperature sensitive procedures like preparation of viable cell extract. In this paper, the optimum tip immersion depth (20-30% height below the liquid surface) is estimated which ensures maximum mixing thereby enhancing thermal dissipation of local cavitation hotspots. A finite element (FE) heat transfer model is presented, validated experimentally with (R^2 > 97%) and used to observe the effect of temperature rise on cell extract performance of E. coli BL21 DE3 star strain and estimate the temperature threshold. Relative yields in the top 10% are observed for solution temperatures maintained below 32°C; this reduces below 50% relative yield at temperatures above 47°C. A generalized workflow for direct simulation using the COMSOL code as well as master plots for estimation of sonication parameters (power input and pulse settings) is also presented.

Topical heading: Transport Phenomena and Fluid Mechanics

Keywords: Cell free protein synthesis, tip-sonication, protein-denaturation, bacterial cell lysis, sonolysis, ultrasonic cell disruption

Introduction

Cell free protein synthesis (CFPS) is a method of producing proteins *in vitro*, which is widely used to manufacture synthetic biology sensors [1–3], prototype proteins [4,5], discover metabolic pathways [6,7], and to manufacture some protein therapies [8–10]. In a typical reaction, the protein is expressed by combining cell extract with energy supplements and a DNA template. Bacterial cells, most commonly a productive *E. coli* strain with protease knockouts (BL21 DE3 star), are lysed to produce the cell extract which contains required intercellular machinery for the reaction, like ribosomes and metabolic enzymes [11]. As an active cell extract is key for optimal CFPS, many groups have focused on optimizing and streamlining the extract production procedure [12,13]. Sonication is a convenient and cost-effective method for lysing small cell batches (<20 g wet cell weight), as opposed to use of more capital-intensive homogenizer or French press at larger scale [12–14].

Sonication uses oscillating ultrasonic waves to lyse the outer membranes of cells via cavitation. A probe transducer [15,16] is inserted into the fluid vessel (Fig 1a) and its tip oscillates causing rapid back and forth fluid motion, leading to pressure waves that create and compress bubbles [17]. The resulting shock waves from collapsing bubbles are sufficient to rupture cell membranes. The local temperature, in a very small region of cavitation, increases by thousands of degrees K [18], but quickly dissipates. Over time this causes buildup of thermal energy in the sonication tube causing temperature rise [15,18]. Additionally, sonication induces fluid flow via ultrasonic waves in a process called acoustic streaming [19]. Proper mixing in the cell suspension vessel is necessary for efficient sonication, to eliminate local hot spots [20]; otherwise a small fraction of suspension

will be over sonicated (causing unwanted temperature rise) and the bulk of the suspension will sit idle. For cells collected from typical shake flask growths (~1-20 g wet cells, prepared at 1 g/ml buffer), sonication is typically performed in snap-cap microcentrifuge 1.5 mL tubes, but can also be done in 5, 15, and 50 mL conical vessels (Fig 1b). Most protocols carefully specify tip height placement or suggest manual motion of the tip to ensure the suspension is mixed and subject to the same level of ultrasonic exposure. The production of viable cell lysate is proportional to cavitation and the extent of cavitation is dependent on the power input [16,18,21]. Higher power density results in faster cell lysis, but greater heat accumulation. Researchers concluded that the total sonication energy input from the tip ultimately converts to thermal energy very near to the tip [22,23]. It is documented that extract conditioning temperature rise affects CFPS yield [24], which agrees with our biophysical understanding of denaturing and loss of function at elevated temperatures, typically > 42◦C [25,26]. It is also observed that prolonged ultrasound exposure can have adverse effects on biological molecules, namely the formation of hydrogen, hydroxide and peroxide radicals and degradation of protein and enzymes [15,27–29].

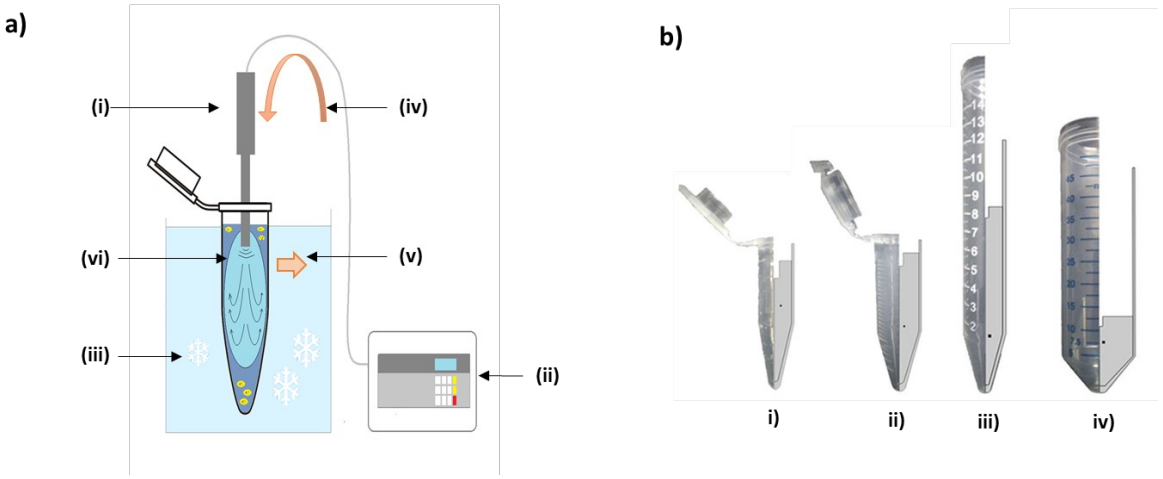

Figure 1 – (a) Schematic depicting cell lysis by tip sonication: (i) sonicator tip is inserted into the sonication vessel, submerging tip in liquid. (ii) Controller for specifying pulse, amplitude & duration iii) The tube sits in ice-bath for cooling iv) Input energy from controller (ii) is set as a function of signal amplitude (translates to tip power based on fluid volume and vessel), pulse durations, and total sonication time v) Thermal energy transfers to ice-bath from cell suspension domain vi) The sonicated liquid is divided into circulated zone & dead zone (b) Axis-symmetric models (right half) of common laboratory tubes: i) 1.5 mL microcentrifuge tube ii) 5 mL microcentrifuge tube iii) 15 mL Falcon tube iv) 50 mL Falcon tube

It is also important to note that adverse temperature effects of sonication extend beyond this paper's focusing example of cell lysate preparation. For example, mass loss of graphene nano particles is caused by temperature rise in sonication [30]. In ultrasonic extraction of corn, overexposure causes reduction of glucose release due to denaturation of enzyme due to temperature rise. There is a reduction in taste, vitamin content and loss of texture in foods that over processed with ultrasonic extraction [31]. In another example, single walled carbon nanotubes (SWCNT) bundle ends are frayed due to temperature rise caused by ultrasonic exposure [32,33]. Thus, a model for mixing and temperature rise caused by sonication will find uses in broader biotechnology applications.

Sonication protocols are designed to mitigate this influence of temperature rise and improve mixing; however, they currently require much empirical testing to determine. Typically, the probe is operated in a pulsed fashion with defined on and off cycles. Additionally, the

sonication vessel is submerged in an ice bath or chiller line. There is a tradeoff between the number of cells lysed and the extract viability which decreases when over-sonicated. From a physical standpoint, it is logical that there exists a threshold temperature for each type of extract, and corresponding sets of optimum parameters to stay below this threshold, but in practice, finding this threshold and controlling temperature rise experimentally can be difficult. The sonicator parameters of input power, pulse durations, and total sonication times are empirically optimized for a given vessel, often necessitating a large number of experiments to cover the design space [13]. Characterization tools can help direct such experiments, but their utility for small volume lysate preparations are limited [21]. The velocity field inside a sonoreactor can be monitored by particle image velocimetry (PIV) techniques [34,35], but for opaque lysate in a small tube such techniques cannot be used to conveniently measure the velocity pattern. It is also difficult to routinely measure temperature in such small volumes by thermocouple and as the vessel is seated in an ice bath, it is also difficult to monitor the inner vessel temperature by NIR imaging. Thus, to more efficiently design optimal sonication protocols for thermally sensitive procedures like cell extract preparation, we propose finite element modeling of mixing and thermal effects.

Finite element modeling of ultrasound systems has been demonstrated in literature, especially for larger reactors. Fluid flow in large sonoreactor (> 500 mL) has been extensively studied [36–38]. The temperature-rise in large reactors, however, is less prevalent, likely due to temperature rise being negligible in a large vessel when subjected to low power density input and having a larger surface area for thermal dissipation [39]. Effects of ultrasound (temperature rise and fluid

streaming) are mostly studied for medical applications of high-intensity, focused ultrasound [40,41]. Conversely, in cell extract preparation, much smaller, laboratory scale tubes (Fig 1b) are used and both mixing and temperature effects will need to be managed. This can be done using a similar framework of finite element modeling.

This paper provides a computational model to predict the effects of tip sonication parameters on mixing and temperature rise in small vessels, commonly used for cell extract preparation. First the relationship between fluid flow patterns and tip immersion depth is modeled; this is used to estimate the optimum tip depth which maximizes mixing. This is done by numerically calculating the stationary velocity field inside the sonication tubes for different tip immersion depths and comparing the fractional volume with regular, circulating streamlines. Next a heat transfer model is used to predict temperature rise over time due to sonication in lab scale tubes which is then experimentally validated. This model is then used to estimate the optimal threshold temperature in a common cell extract strain (BL21 DE3 star) using optimized CFPS experiments presented in literature [13]. This model coupled to experimental data can then provide insight on the effect of sonication temperature on cell lysis yield. A stepwise workflow is then presented for use of these numerical models in obtaining optimized parameters for other novel sonication set ups. Lastly, we provide convenient master-plots for determination of optimal sonication conditions for new temperature thresholds without need of running the modeling code.

Result and Discussion

1) Effect of sonication tip position on extent of mixing

Before determining thermal effects of sonication, a simple acoustic streaming model is used to study the effect of sonication tip position on extent of mixing. A tip placement that induces near to complete mixing is necessary to simplify the heat transfer model (assumption of uniform mixing, decoupling acoustic model from thermal). From our finite element model (see methods), we obtain stationary flow velocities at each point inside the sonication tube. As estimated from other literature sources [42], it is observed that the liquid flows as a uniform jet downward from the sonicator tip, gets deflected by the bottom of the vessel and flows upward, turning near the vessel neck back towards the tip creating a circulation zone of rotating streamlines (yellow color in Fig 2a). Outside the circulation zone there are two regions with moderate to low, irregular velocity ('dead zones' at the top and bottom of the tube, indicated by the grey area in Fig 2a). Our goal is to maximize the circulation zone and reduce the dead zone in each tube based on tip position.

This simulation was run for different tip depths starting at 0.5 cm and increasing at intervals of 0.5 cm for each of the four standard tube sizes used in tip sonication of cell extract (1.5, 1.5, 5, 15 and 50 mL) with volumes of 1.5, 1, 5, 10, and 15 mL respectively. Simulation results are shown as streamline diagrams, indicating the boundary of the circulation zone in each of the four tubes (1.5 mL diagram is shown in Figure 2, remainder can be found in Supplementary Fig

1-5). The circulation zone fraction to total fluid volume is quantified with ImageJ and percent circulation zone is plotted as function of tip immersion depth from surface percentage to total liquid depth. It is observed that for each of the tubes simulated the greatest percentage of volume is mixed, if the tip depth is within 20-30% from the top of the total liquid height and is best mixed in a 50 mL tube (with 15 mL total volume).

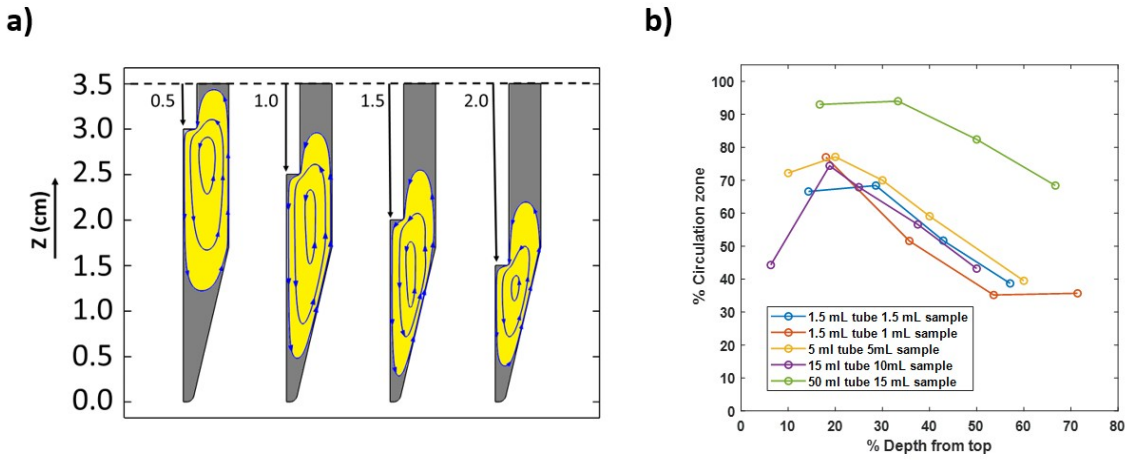

Figure 2: Modeling effect of tip depth on mixing. a) Circulation zone (yellow) and dead zone (gray) with different tip depths for 1.5 mL Microcentrifuge tube obtained from simulation. b) Percentage of volume in circulation zone with changing tip height for four sizes of tubes 1.5,1.5, 5, 15, and 50 mL with 1.5,1, 5, 10, 15 mL sample respectively.

For the common 1.5 mL snap-cap microcentrifuge tubes the vessel cavity is narrow (low clearance between tip and wall) and the liquid has a smaller circulation zone; when the tip depth is more than 60% of the liquid height, the circulation zone percentage falls below 50% of

the total capacity, in simulation. Another interesting observation is reduced mixing at the shallower tip depths for the 15 mL centrifuge tube; this tube has the highest length to diameter aspect ratio of the tubes screened and we observe a dead zone build up at bottom of the tube if the depth is less than 20% from the top; likewise, there is reduced mixing if depth is more than 40% (dead zone near the top surface). The 50 mL tube is the only one simulated that can achieve nearly 100% mixing (at depths less than 40% total fluid height). We attribute this to the superior circulation zone observed in this vessel size. However, the 50 mL tube has the limitation of poorer heat dissipation (smaller area to volume ratio) leading to greater potential of heat build-up and damage to cell extract preparation. This laminar model does not take into account the improved mixing cause by turbulent eddies caused by sonication; thus we progress to the heat transfer model by making the assumption of complete mixing for all tubes and then use experimental validation to confirm use of this assumption.

2) Heat transfer model and experimental validation

Temperature rise due to sonication was simulated using a finite element heat transfer model (see methods) for four sets of pulse length, total power, and vessel size conditions: (1) 10 s, 5.5 W, 1.5 mL, (2) 20 s, 5.5 W, 1.5 mL, (3) 10 s, 12.5 W, 5 mL, (4) 10 s, 1.73W, 1.5 ml tubes. These were then experimentally validated under the same conditions using a thermocouple probe (Fig 3, supplementary figure 9). It is observed that the simulated temperature profile matches well with the experiment (R^2 = 0.9947, 0.9989, 0.9926 and 0.9849). This indicates that the model

assumptions made (namely complete mixing in the tube) are adequate and that the model can be used to assess published data and to calculate optimized conditions.

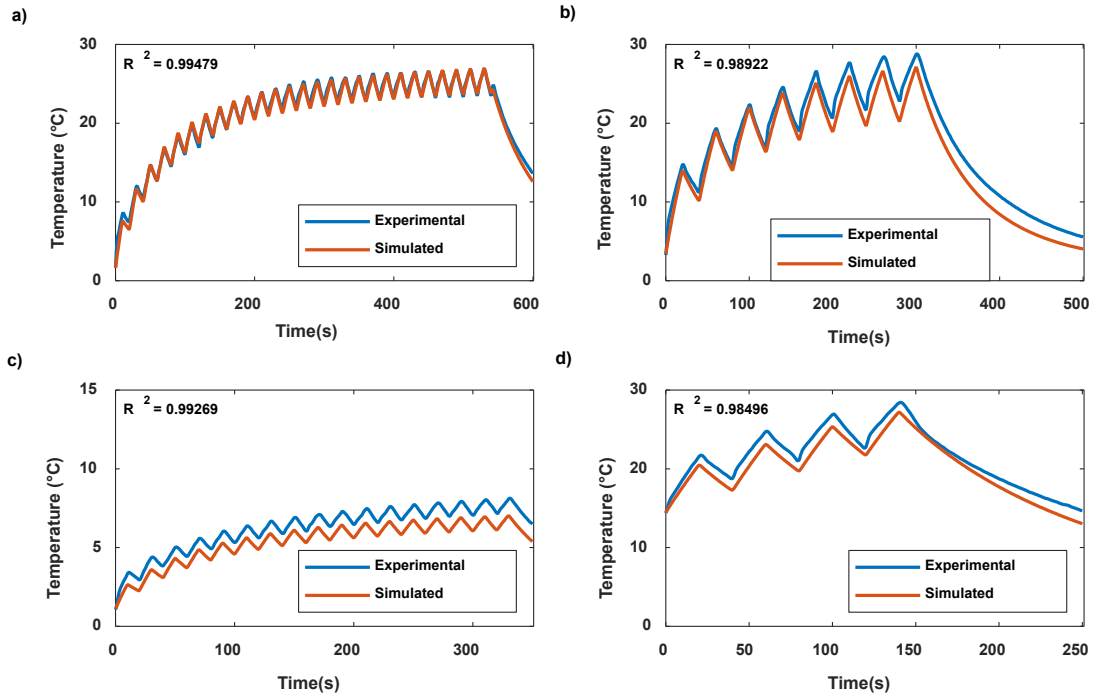

Figure 3 - Temperature rise over time determined experimentally (blue line) and estimated with the finite element simulation (orange line). a) 1.5 mL microcentrifuge tube with 1.5 mL sample at 50% amplitude using a 3mm tip (corresponding to ~5.5 Watt) and 10 second on and 10 second off pulse, initial temperature 1.6◦C. b) 1.5 mL microcentrifuge tube with 1.5 mL sample at 50% amplitude using a 3mm tip (corresponding to ~5.5 Watt) and 20 second on and 20 second off pulse, initial temperature 3.4◦C. c) 1.5 mL microcentrifuge tube with 1.5 mL sample at 25% amplitude using a 3mm tip (corresponding to ~2 Watt) and 10 second on and 10 second off pulse, initial temperature 1.1◦C. d) 5 mL microcentrifuge tube with 5 mL sample at 50% amplitude using a 6mm tip (corresponding to ~12.5 Watt) and 20 second on and 20 second off pulse, initial temperature at 14.4 ◦C.

From the model and experimental data, we observe that the temperature starts rising immediately as the sonication starts and within a relatively short time (300-500 s) it reaches a steady state, a point where the energy added by sonication is equal to the energy lost to the ice-bath. It is also observed that the temperature follows a very predictive parabolic pattern while rising and the model could capture this effect. The model can then be used to estimate temperature rise for different sonication conditions with different power input, vessel geometry, sample volume and pulsing.

3) Estimation of optimum temperature in cell extract preparation & role of power density

With a valid heat transfer model in place, we can next estimate the maximum temperature threshold during cell lysis for optimum yield from the common *E. coli* BL21 DE3 star strain. This can be estimated using the published data by Kwon et al. [13] where relative CFPS yields were measured from 144 samples of extract prepared by sonication at different volumes (1500, 1000, 700, 500, 300, and 100 µL) and input energy; other parameters such as sonication amplitude, tip size, pulse on duration, and pulse off duration were held constant at 50%, 3 mm, 10 s, and 10 s respectively and the tube was cooled by an ice bath, starting at 277K. From this, a contour map was produced by plotting energy added (x-axis), volume of sample (y-axis) and yield (z-axis) (reproduced from original data in Fig 5a). This plot shows the effect of sample volume and energy added on yield.

To convert this data to temperature, we first needed to determine the power input for each of the sample volumes. We empirically determined the power at each of the measured volumes using the same sonicator (Qsonica 125) set at 50% amplitude (Supplement Fig 6,7), observing that the power input at a given amplitude setting on the sonicator is dependent on the volume of the liquid. This measured input power was then divided by the sample volume to get the volumetric heat source used in the heat transfer model (Q_g term, discussed in methods). The pulse time (10 s on and off), cooling condition and all associated geometric and thermal parameters were supplied as model inputs according to the simulation outlined in the methods section. Using the model, the temperature is estimated over time for each volume. The peak temperature in a cycle of on-off pulses is observed at the last second of the on pulse (Fig 3, top of each saw tooth wave). From the temperature vs. time data, we select the temperature at each peak and convert the sonication time data (cumulative of pulse on time only) to energy by multiplying with the effective power value. By this we obtain temperature vs. energy data and interpolate to determine the temperature value for a given input energy value (over the range of 0 to 1600 Joules used by Kwon et al., see Supplement table 16 for example calculation). This data is then used to create a temperature matrix (supplementary table 17,18) and this data is superimposed as contour lines on the same yield plot from Kwon et al. (Fig 4a). Temperature and normalized yield for individual sample volumes are also plotted in Supplementary Figure 8.

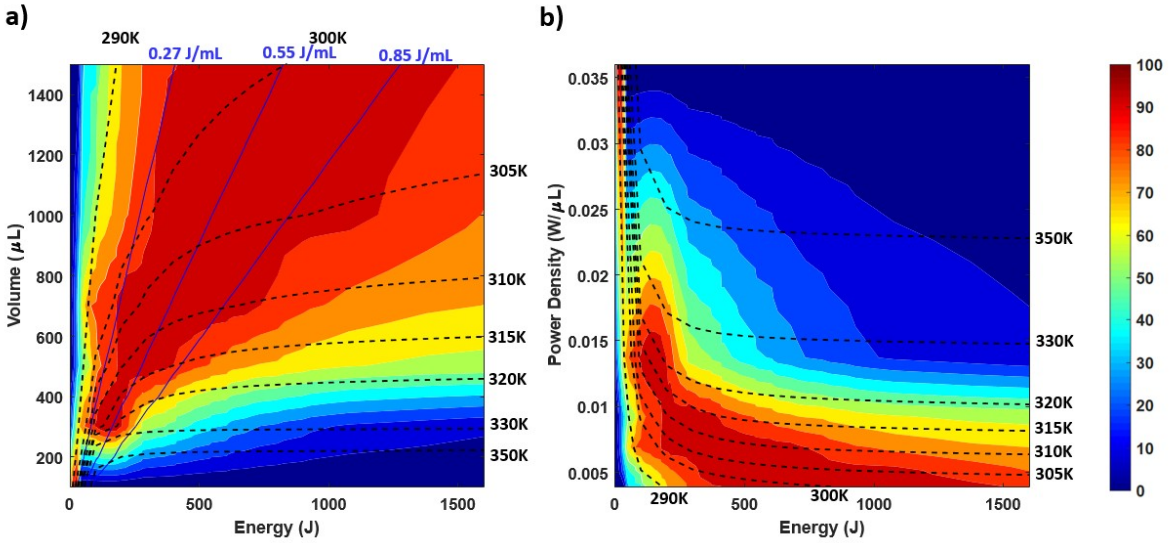

Figure 4 – a) Heat map of normalized sfGFP yield from BL21 DE3 Star cell extracts prepared at different volumes and total energies, with z-axis color bar presenting relative amounts of expression (replotted from [13]). Thick dashed lines depict temperatures (K) at these sonication conditions obtained by the finite element simulation. Thin solid lines indicate energy density values (J/mL). b) The same normalized yield data plotted in a more generalized fashion as power density vs. total energy; dashed lines again show temperatures estimated by simulation.

These modeled temperatures allow us to observe the effect of temperature on different yields. From the graph, it can be observed that the yield is > 90% relative yield in regions where temperature is below 305K; beyond 320K the yield reduces below 50% relative yield. Our finding that protein yield is influenced by temperature is well supported by cell free literature [24]. We also observe from the Kwon data that increased energy at larger volume has little effect on yield; this is again attributed to temperature effect as we see from the model that the

mixture reaches a steady state temperature below the 305K limit. Again, the steady state is reached when the heat added by sonication and removed by cooling is equal, which depends on rate of energy supplied, as we discuss next.

In the Kwon et al. study, a linear equation is presented that determines total energy needed based on sample volume to optimize protein yield, but this is only at a set specific amplitude and pulse on/off times. It makes intuitive sense that the yield is not only dependent on total energy supplied per volume (energy density), but also the rate at which energy is supplied per unit volume (power density and pulsing times). In the Kown et al. framework a certain amount of energy has to be given per volume for optimal lysing. However, the energy could be supplied slowly (less power density and short pulse on time) or quickly (more power density long pulse on time). Intuitively, if the energy is supplied too fast the temperature would rise above an undesired point, and the yield should fall. This power density effect can be studied with the heat transfer model. For example, the optimum energy for a 1000 µL sample according to the Kwon et al. equation is (1000-33.4) $\times$ 1.8^{-1} = 553 Joules. If this 553 Joules is supplied using 15 Watt power corresponding to 0.015 W/µL power density with 20 second on-off pulse, it would take only two bursts to supply the required energy and the total processing time required would be one minute; however, the final temperature would be above 340K and yield would suffer despite use of the optimal energy density.

Thus, to observe the role of power density more clearly, we transform the same data into another contour plot (Fig 4b). Here the y-axis is changed from volume to power density by

dividing the tip input power at that liquid volume (empirically derived – Supplement figure 7) by the volume. The x and z-axis are kept the same as before (energy and yield, temperature values respectively). At these sonication conditions (50% amplitude and 10 s pulse settings) the relative yield is above 90% in the small window of power densities between 0.005 to 0.01 W/µL and 200 to 1000 J total energy. If the power density is more than 0.015 W/µL, the yield is low (<60%) regardless of energy input and the modeled temperature increases above 320K for total energies above 100 J. Another interesting observation from inspecting the data in terms of power density, is that at each power density the temperature rises to a steady state very quickly (horizontal isotherms). This means that at each sonication setting (under active cooling, ice bath) the steady state temperature can be determined by the finite element heat transfer model. In other words, the maximum temperature that can be reached in a sonication system can be tuned using the heat transfer model by altering power density and pulsing.

4) Optimizing temperature sensitive sonication using the heat transfer model

The finite element heat transfer model (COMSOL code in Supplement section 11, also as a module) is readily adaptable and can be used to efficiently determine optimal sonication settings for new temperature sensitive processes. For cell-free extract, this could be using a different sonication vessel, cooling method, or cell extract density. This also has utility beyond cell-free, such as preparation of temperature sensitive emulsions, nanoparticles, or nano-sensors in which the same model can predict temperature rise (after adjusting fluid intrinsic properties). This can be done in a logical stepwise process (summarized in Fig 5).

First, the vessel materials and associated thermal parameters, vessel geometry, sample volume, cooling method (water bath, ice water bath, ice water bath with cooler, insulation or no cooling) are specified as scalar values and proper boundary conditions within COMSOL. The energy requirement per volume is determined according to process requirement (*e.g.* for cell extract, the energy needed to lyse the cells). In most cases, this is done by empirical measurement. For cell lysis of BL21 DE3 cells, the Kwon et al. data shows yield > 90% lies between 0.27 J/μL to 0.85 J/μL (solid blue slopes shown on Fig 5a). In our model the midpoint, optimal energy density of 0.55 J/μL is used.

Next, the minimum power density and threshold temperature for the specific sonication task should also be specified. In cases of larger volume sonication, if the power density is too low there will not be sufficient power to cause cavitation (and thereby lysis of cells, formation of nanoparticles, etc.) [43]. Again, one estimates the minimum power density from process knowledge or empirical data, but this is used as a starting point for the simulation and is adjusted to meet the target threshold temperature (which is again found empirically). For BL21 DE3 star cells, good yield was obtained using a power density between 0.003 and 0.01 W/μL.

The optimum power density and pulse time is obtained iteratively from the model. First the duration of sonication is calculated using the equations in the third process model block (Fig 5) using an initial guess of power density higher than minimum and set pulsing times. The FE model is then used to calculate temperature rise over time. If temperature surpasses the

threshold, the power density and pulsing are changed (less power, shorter pulses to drop temperature) and the simulation is again repeated until pulse timing and set power density is obtained for which temperature is below threshold.

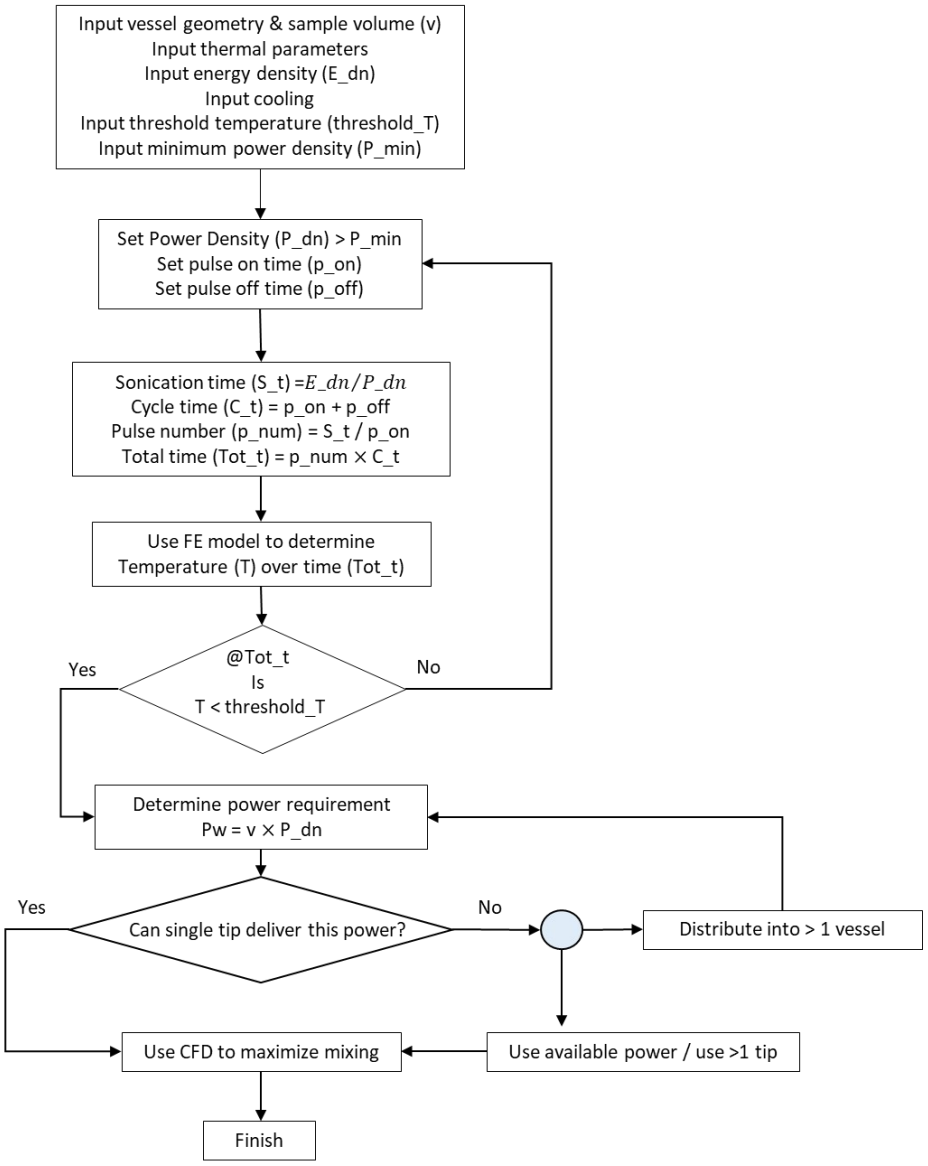

Figure 5: Workflow diagram to obtain optimized sonication parameters for temperature sensitive procedure using the finite element model directly (access to COMSOL required to run provided process code).

Next, the total power requirement is calculated by multiplying the power density used in the model with the sample volume. If a single tip is not capable of supplying this total power (10 and 17 W from the 2 and 3 mm QSonica tips) the sample can be divided into more than one tube or a larger tip can be used (however, this again affects the model geometry which takes into account total fluid and tip size). After the input power is selected, the mixing is optimized by using the CFD calculation by adjusting the sonicator transducer position using the geometrical and fluid parameter in the first block. Installing baffles could enhance mixing but is beyond the scope of this simple model.

With this workflow one can obtain a set of optimized sonication parameters, namely transducer position, power density, pulsing and sonication duration that will ensure better mixing and safe temperature rise. This same workflow is applicable to other geometries such as a sonication bath in beakers, automated sonication systems, or miniature lab on a chip cell lysis device (making sure to change geometry of the model and correctly specifying the sonication transducer surface). However, this iterative process requires resources to run the finite element model, and in the case of tip-sonication of cell extract, a set of master data would be sufficient to interpolate most process conditions, without need of solving the finite element equations.

5) Optimizing sonication with master plots for common cell extract parameters

Noting that both software access and computation time necessary to run our finite element model may limit its utility, we also devised a set of master plots that can likewise be used to efficiently select sonication conditions for cell extract processing, but still gives the flexibility to use strains that have different temperature and power density limitations. Here we model the maximum temperature that can be reached in aqueous samples by a standard tip sonication set up (cooling in ice-bath with sufficiently large volume) for four common sonication tube sizes, while varying power density and pulse settings (Fig 6). These plots can be used directly to find optimal sonication parameters at a set temperature threshold without having to run the FE model.

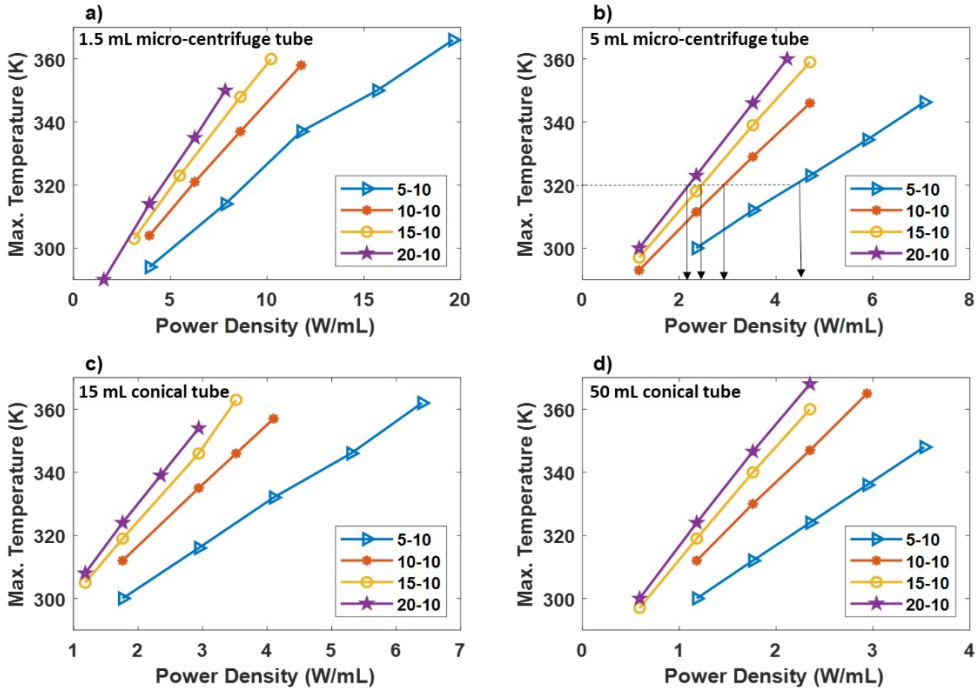

Figure 6: Maximum temperature (y-axis) estimated for different power density (x-axis) and pulse time (5-10,10-10,15-10 and 20-10 on-off pulses respectively) for each of the four tubes – a) 1.5 mL microcentrifuge tube b) 5 mL microcentrifuge tube c) 15 mL conical tube d) 50mL conical tube.

To provide clarity on use of these master plots we provide an example. Assume a cell growth yields 3 g of cells, to make 3 mL of cell suspension for sonication and the specific strain threshold temperature is 320K (empirically observed). First a sonication tube with adequate volume is selected – in this case the 1.5 mL tube is too small, and the 5 mL tube is a suitable choice. Next, draw a horizontal line at the max temperature (in this case 320K) for the selected tube (dotted line in Fig 6b) which will intersect lines for four different pulse condition (5-10,10-10,15-10 and 20-10 on off pulses). The power density for these pulse conditions are then read from the x-axis at these points (4.5, 3, 2.5, and 2.2 W/mL respectively). Then the sample volume (in mL) is multiplied with the power density for the selected pulse condition to get the maximum permissible power. In the case of 3 mL samples in the 5 mL tube at the 5-10, 10-10, 15-10 and 20-10 s on/off pulse settings, the max power settings obtained are 13.5, 9, 7.5, 6.6 W respectively. Now one can tune the power setting with reference to the sonicator calibration chart (provided by vendor or empirically determined, see Supplement Fig 6,7) to select an input power that will not exceed the threshold temperature. In the case of this example, if less than 6.6 W power is used with 20-10 s on/off pulses the maximum temperature will always be below 320K regardless of time sonicated. The next step would be to process a few batches of cells at these conditions to determine the appropriate energy density (J/mL) and thus overall length of

sonication (number of pulse) cycles on yield. Using the optimal energy density of 550 J/mL from the BL21 DE3 star cells, the sonication duration would be 570 seconds or 19 cycles.

Conclusion

The optimum tip immersion depth which facilitates mixing is estimated from the relationship between fluid flow pattern and tip position using a simplified acoustic streaming model. A time dependent heat transfer model is also presented which can estimate temperature rise in laboratory scale sonication given process inputs. Assumptions were made and validated by experiments which enabled us to decouple heat transfer model from acoustic pressure and velocity distribution. Using the model and previous experimental data, effect of temperature on yield of BL21 DE3 Star strain is calculated. The model offers us process insight on how input parameters like power, sample volume and pulse time affects temperature rise. This model can also be used to tune the parameters to control temperature in other lab scale sonication procedures like extraction of biological and food samples where temperature rise is a concern; this model allows one to narrow in on a range of suitable power and pulse setting without the need for lengthy iterative laboratory experiments. Use of this model can be extended to any tip sonicator, irrespective of vendors, by empirically determining input power as a function of amplitude setting and volume. Although this model is used for laboratory scale tubes, in future work, it could also be applied for scale up in larger vessels. Finally, the central finding of an optimal temperature range for cell extract preparation can be used in design of a closed loop sonication system with real time temperature control.

Methods

Simulations were conducted as axisymmetric models (2D interface) in COMSOL multiphysics 5.4. To find model dimensions, the sonication tubes were dismantled, and height, thickness, and width were measured with slide calipers. The model was then drawn directly in the COMSOL computer aided design interface with specified acoustic and flow boundary conditions (Fig 7, Table 1,2,3). The sonication tubes as well as tips are cylindrical and can be represented by taking half of the cross section along the mid plane (axisymmetric geometry). Finite element analysis demands the simulation domain to be discretized to number of elements, and the solution is obtained at each of the nodes.

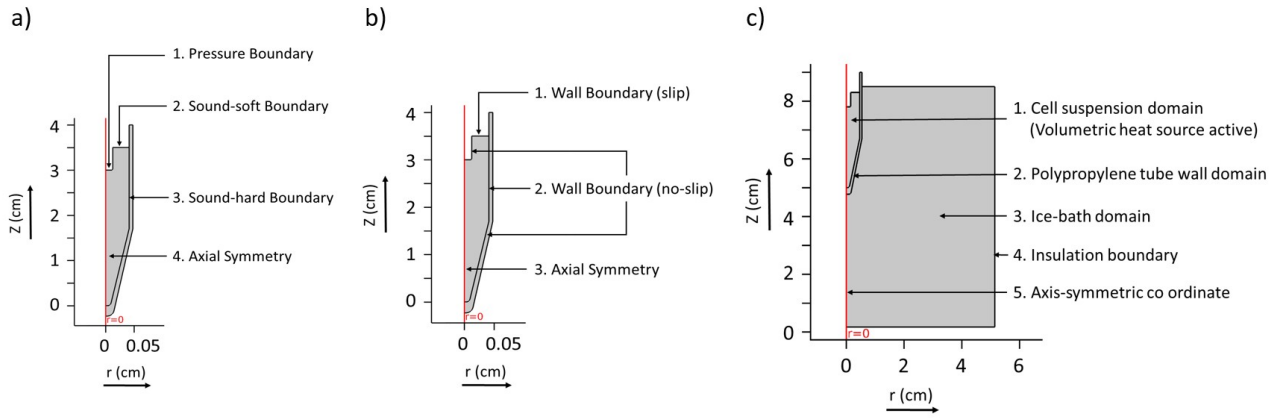

Figure 7: Model drawing in COMSOL with specified boundary conditions for a) Pressure acoustics, b) Laminar flow and c) Heat transfer

Table 1 - Pressure Acoustic Boundary Conditions

Index	Domain and Boundary condition	Equations
1. Boundary	Pressure Boundary	P = Po
2. Boundary	Sound soft boundary	- n.¿P) = 0
3. Boundary	Sound hard boundary	P_t = 0
4. Boundary	Axis-symmetric coordinate	r = 0

Pressure acoustics and laminar flow modelling

The pressure distribution in a system can be calculated by inhomogeneous Helmholtz equation:

$$\nabla . \left[\frac{-1}{\rho_c} (\nabla P) \right] - \frac{\omega^2}{\rho_c C_c^{\,2}} P = 0 \qquad \text{[Eq. 1]}$$

where *P* is the acoustic pressure of the media. The angular frequency ω is defined as $\omega = 2\pi f$, where *f* is the ultrasound frequency.

ρ_c and C_c is the complex density and complex sound speed, respectively. They can be expressed by the following equation as –

$$\rho_c = \frac{\rho C_s^{\,2}}{C_c^{\,2}} \text{ and} \qquad \text{[Eq. 2]}$$

$C_c = \frac{\omega}{k_c}$ [Eq. 3]

Where ρ and *Cs* are density of the medium and sound speed, respectively. Complex wave number k_c can be expressed as:

$k_c = \frac{\omega}{C_s} - i\alpha$ [Eq. 4]

Where C_s and α are the sound speed and absorption coefficient in the media respectively.

The input pressure is calculated by equation [5] -

$P_0 = \sqrt{(2\rho C_s I)}$ [Eq.5]

Where 'I' is the intensity of the sound. It is assumed that all the power enters the tube through the tip of the transducer. The power input P_w is in watts. Intensity is given by,

$I = \frac{P_w}{A}$ [Eq. 6]

Where A is the area of tip (30.2mm^2 for the standard 1/8" or 3mm diameter sonication tip). In this study the input power is set at 5.5 W because this is corresponding to power delivered by a Qsonica 125 with 50% amplitude with 3.1 mm diameter sonication tip which is the usual

sonication parameter for cell lysis. In cavitating media, the absorption coefficient is very high and difficult to determine [44]. For the purpose of this study the absorption coefficient of the media is considered 1 m^{-1} for water adopted from Xu [37]. All the input parameters are listed in (Supplement table 1). Solving the stationary Helmholtz equation [Eq.1] gives pressure at each point of the simulated tube. From the resulting pressure field, the intensity field can be calculated using equation [5].

The stationary laminar flow field is modelled by two equations- 1. The momentum balance equation [Eq. 7] and 2. The continuity equation [Eq. 8]:

Index	**Domain and Boundary condition**	**Equations**
1. Boundary	Wall Boundary (slip)	-n.u= 0
2. Boundary	Wall Boundary (no slip)	u = 0
3. Boundary	Axial Symmetry	r = 0
4. Domain	Volumetric Force	F = $\frac{2\alpha I}{\rho C}\frac{N}{m^3}$

Table 2 - Laminar Flow Boundary Conditions

$$\rho(\vec{u}.\nabla)\vec{u}=\nabla.[-PI+k]+F \qquad \text{[Eq. 7]}$$

$$\rho\nabla.\vec{u}=0 \qquad \text{[Eq. 8]}$$

Where $\rho, \vec{u}, P, I, k \wedge F$ are fluid density, velocity vector, fluid pressure, identity tensor, fluid viscosity and volumetric force respectively.

The volumetric force term (*F*) in momentum balance is calculated from the pressure intensity field $I,$ determined from Eq. 9. Assuming plane wave approximation *F* can be expressed by the following relationship:

$$F = \frac{2\alpha}{C_s} I \qquad \text{[Eq. 9]}$$

Detail of this derivation can be obtained from [45].

Where *F*, α , C_s and I are volumetric force, sound attenuation coefficient, sound speed and intensity, respectively. Solving this with finite element analysis in COMSOL using the specified boundary conditions (Table 2) and input parameters (Supplementary table 2) yields the velocity field at each point of the sonication tube (Fig 7b). Velocity streamline indicates the direction of fluid flow. The area inside the streamlines are marked yellow and quantified with ImageJ. (details in supplementary figure 1-5, table 3- 12)

Temperature modeling simulation

Temperature rise due to sonication is modelled using the 'Heat transfer in solid and fluid interface' module in COMSOL Multiphysics v5.4 as a time dependent study. The simulated model has three domains (Fig 7c): 1) sonication tube domain, 2) polypropylene tube wall

domain, and 3) ice bath domain. The thermal and physical properties of each of the domains is listed in supplement (Supplement Table 13).

The time dependent heat transfer equation is:

$$\rho_s C_p \frac{\partial T}{\partial t} = \kappa_s \nabla^2 T + \rho_s C_p \vec{u} \ \nabla . T + ¿Q_g + ¿Q_{loss} \qquad \text{[Eq. 10]}$$

Where ρ_s, C_p, T, k_s, $\vec{u}$, Q_g and Q_s are domain material density, specific heat, temperature, thermal conductivity, velocity vector, heat generation term and heat loss term, respectively.

Returning to the velocity field solution above, the assumption of laminar flow should not be used for this calculation, only for generalization of fluid volume affected by the tip (Fig 2). Rather, in an extremely turbulent environment with nonlinear cavitation constrained to a small cavity it is difficult to determine the time dependent velocity field coupled with heat transfer. Due to turbulence, there is a time-dependent change in thermal properties such as the thermal conductivity ‘k’. Due to high conductivity, small scale and assumed complete turbulent mixing, the cell suspension domain is considered isothermal and the velocity term can be neglected. This simplifies the heat transfer in the tube to the following equation –

$$\rho_s C_p \frac{\partial T}{\partial t} = \kappa_s \nabla^2 T + ¿Q_g \qquad \text{[Eq. 11]}$$

The ice-bath is considered large enough so that it can effectively act as a heat sink without much temperature rise. The material and thermal property of ice bath is assumed similar to ice. The total outside domain can be considered insulated (no heat flow in or out) as outside temperature has negligible effect in temperature of the domains.

The heat generation term Qg is active only inside the sonication tube domain as a volumetric heat source in W/m^3. The power delivered is measured empirically from the sonicator and multiplied with a tip conversion factor to account for realistic loss of power of 0.85 from literature [46] and divided by the sample volume to get the volumetric heat source term. The volumetric heat source is multiplied by a piecewise time function to incorporate pulsing. The function value is 1 while the pulse is on and 0 when pulse is off. Temperature value is stored for each second.

Table 3 Heat Transfer Boundary Conditions

Index	**Domain and Boundary condition**	**Equations**
1. Domain	Cell suspension domain (volumetric heat source active, isothermal)	$Q_g = \frac{Input\ Power \times conv.factor}{sample\ volume}$
2. Domain	Tube wall domain (tube material – polypropylene)	
3. Domain	Ice-bath domain	
4. Boundary	Insulation	n.q = -n.q = 0
5. Boundary	Axial Symmetry	r=0

Experimental Temperature measurement for Model Validation

Cell suspensions are prepared as described before [47]. In brief, starter culture is prepared by taking 20 mL of LB media (prepared by protocol outlined in [2]) and a cell pick of BL21 DE3 Star. This starter culture is left to grow overnight and used to inoculate 1 L growth media of 2x YTPG (prepared by protocol outlined in [2]) in a 2.5 L Tunair flask. The cells are harvested after 4 hours. The cell pellets are resuspended in S30 buffer, centrifuged (at 3000g for 20 minutes in 4◦ C temperature) and pelleted again. These cells are mixed with equal volume of S30 buffer and vortexed to produce cell suspension which is aliquot in tubes.

The sonication tubes are placed in an ice bath containing ground ice in water, stabilized with a clamp. The sonication tip is dipped in the suspension 0.5 cm from top as per the optimum depth found from this study (Fig 2). A k-type probe data logger thermometer (Fluke TC-2000) is used for temperature measurement and logging. The probe head was carefully held manually inside the sonication tube so that it did not touch the tube wall or the sonication tip due to vibration. The amplitude and pulse settings were specified and the sonication and data logging was started at once. The experiments were conducted with different power setting, pulse setting, tip radius, tubes and initial temperatures to observe the experimental response in different conditions and validate the finite element model. For each of the experimental runs, simulations were also conducted using the model inputs. The experimental runs were -

1. 1.5 mL microcentrifuge tube with 1.5 mL sample & 50% amplitude 3mm tip (corresponding to 5.5 Watt) and 10 second on and 10 second off pulse, initial temperature 1.6 ◦C. (Fig 3a)

2. 1.5 mL microcentrifuge tube with 1.5 mL sample & 50% amplitude 3mm tip (corresponding to 5.5 Watt) and 20 second on and 20 second off pulse, initial temperature 3.4 ◦C. (Fig 3b)
3. 1.5 mL microcentrifuge tube with 1.5 mL sample & 25% amplitude 3mm tip (corresponding to 1.73 Watt) and 10 second on and 10 second off pulse, initial temperature 1.1 ◦C. (Fig 3c)
4. 5 mL microcentrifuge tube with 5 mL sample & 50% amplitude 6mm tip (corresponding to 12.5 Watt) and 20 second on and 20 second off pulse, initial temperature 14.4 ◦C. (Fig 3d)

Acknowledgements

We thank Prof. Kwon for sending us original sonication data to fit to our thermal model in Figure 4.

References

1. Pardee K, Green AA, Takahashi MK, et al. Rapid, Low-Cost Detection of Zika Virus Using Programmable Biomolecular Components. *Cell*. 2016;165(5):1255-1266. doi:10.1016/j.cell.2016.04.059
2. Salehi ASM, Shakalli Tang MJ, Smith MT, et al. Cell-Free Protein Synthesis Approach to Biosensing hTRβ-Specific Endocrine Disruptors. *Anal Chem*. 2017;89(6):3395-3401. doi:10.1021/acs.analchem.6b04034
3. Takahashi MK, Tan X, Dy AJ, et al. A low-cost paper-based synthetic biology platform for analyzing gut microbiota and host biomarkers. *Nat Commun*. 2018;9(1):1-12. doi:10.1038/s41467-018-05864-4
4. Dopp JL, Rothstein SM, Mansell TJ, Reuel NF. Rapid prototyping of proteins: Mail order gene fragments to assayable proteins within 24 hours. *Biotechnol Bioeng*. 2019;116(3):667-676. doi:10.1002/bit.26912
5. Dopp JL, Reuel NF. Simple, functional, inexpensive cell extract for in vitro prototyping of proteins with disulfide bonds. *Biochem Eng J*. 2020;164:107790. doi:10.1016/j.bej.2020.107790
6. Jaroentomeechai T, Stark JC, Natarajan A, et al. Single-pot glycoprotein biosynthesis using a cell-free transcription-translation system enriched with glycosylation machinery. *Nat Commun*. 2018;9(1):1-11. doi:10.1038/s41467-018-05110-x
7. Dudley QM, Nash CJ, Jewett MC. Cell-free biosynthesis of limonene using enzyme-enriched Escherichia coli lysates. *Synth Biol*. 2019;4(1):1-9. doi:10.1093/synbio/ysz003

8. Zawada JF, Yin G, Steiner AR, et al. Microscale to manufacturing scale-up of cell-free cytokine production-a new approach for shortening protein production development timelines. *Biotechnol Bioeng*. 2011;108(7):1570-1578. doi:10.1002/bit.23103
9. Yin G, Garces ED, Yang J, et al. Aglycosylated antibodies and antibody fragments produced in a scalable in vitro transcription-translation system. *MAbs*. 2012;4(2):217-225. doi:10.4161/mabs.4.2.19202
10. Cai Q, Hanson JA, Steiner AR, et al. A simplified and robust protocol for immunoglobulin expression in Escherichia coli cell-free protein synthesis systems. *Biotechnol Prog*. 2015;31(3):823-831. doi:10.1002/btpr.2082
11. Smith MT, Wilding KM, Hunt JM, Bennett AM, Bundy BC. The emerging age of cell-free synthetic biology. *FEBS Lett*. 2014;588(17):2755-2761. doi:10.1016/j.febslet.2014.05.062
12. Shrestha P, Holland TM, Bundy BC. Streamlined extract preparation for Escherichia coli-based cell-free protein synthesis by sonication or bead vortex mixing. *Biotechniques*. 2012;53(3):163-174. doi:10.2144/0000113924
13. Kwon YC, Jewett MC. High-throughput preparation methods of crude extract for robust cell-free protein synthesis. *Sci Rep*. 2015;5:1-8. doi:10.1038/srep08663
14. Dopp JL, Reuel NF. Process optimization for scalable E. coli extract preparation for cell-free protein synthesis. *Biochem Eng J*. 2018;138:21-28. doi:10.1016/j.bej.2018.06.021
15. Islam MS, Aryasomayajula A, Selvaganapathy PR. A review on macroscale and microscale cell lysis methods. *Micromachines*. 2017;8(3). doi:10.3390/mi8030083
16. Harrison STL. Bacterial cell disruption: A key unit operation in the recovery of intracellular products. *Biotechnol Adv*. 1991;9(2):217-240. doi:10.1016/0734-

9750(91)90005-G

17. Jamshidi R. Modeling and Numerical Investigation of Acoustic Cavitation with Applications in Sonochemistry. Published online 2013:159.

18. Wang M, Yuan W, Hale A. Three-Dimensional Simulation of Ultrasound-Induced Microalgal Cell Disruption. *Appl Biochem Biotechnol*. 2016;178(6):1184-1195. doi:10.1007/s12010-015-1937-z

19. Nyborg WL. Acoustic Streaming due to Attenuated Plane Waves. *J Acoust Soc Am*. 1953;25(1):68-75. doi:10.1121/1.1907010

20. Zhou J, Tada Y, Kato Y, et al. Effect of Mixing on Sonochemical Reaction in a Sonoreactor. *J Chem Eng JAPAN*. 2010;43(8):657-660. doi:10.1252/jcej.09we235

21. Sutkar VS, Gogate PR. Design aspects of sonochemical reactors: Techniques for understanding cavitational activity distribution and effect of operating parameters. *Chem Eng J*. 2009;155(1-2):26-36. doi:10.1016/j.cej.2009.07.021

22. Chivate MM, Pandit AB. Quantification of cavitation intensity in fluid bulk. *Ultrason - Sonochemistry*. 1995;2(1):19-25. doi:10.1016/1350-4177(94)00007-F

23. Prabhu A V., Gogate PR, Pandit AB. Optimization of multiple-frequency sonochemical reactors. *Chem Eng Sci*. 2004;59(22-23):4991-4998. doi:10.1016/j.ces.2004.09.033

24. Kigawa T, Yabuki T, Matsuda N, Matsuda T, Tanaka A, Yokoyama S. E.Coli_cell_free_system_protocol. Published online 2004:63-68.

25. Farewell A, Neidhardt FC. Effect of temperature on in vivo protein synthetic capacity in Escherichia coli. *J Bacteriol*. 1998;180(17):4704-4710. doi:10.1128/jb.180.17.4704-4710.1998

26. de Groot NS, Ventura S. Effect of temperature on protein quality in bacterial inclusion bodies. *FEBS Lett*. 2006;580(27):6471-6476. doi:10.1016/j.febslet.2006.10.071

27. Miller MW, Miller DL, Brayman AA. A review of in vitro bioeffects of inertial ultrasonic cavitation from a mechanistic perspective. *Ultrasound Med Biol*. 1996;22(9):1131-1154. doi:10.1016/S0301-5629(96)00089-0

28. Rokhina E V., Lens P, Virkutyte J. Low-frequency ultrasound in biotechnology: state of the art. *Trends Biotechnol*. 2009;27(5):298-306. doi:10.1016/j.tibtech.2009.02.001

29. Save SS, Pandit AB, Joshi JB. Use of hydrodynamic cavitation for large scale microbial cell disruption. *Food Bioprod Process Trans Inst Chem Eng Part C*. 1997;75(1):41-49. doi:10.1205/096030897531351

30. Baig Z, Mamat O, Mustapha M, Mumtaz A, Munir KS, Sarfraz M. Investigation of tip sonication effects on structural quality of graphene nanoplatelets (GNPs) for superior solvent dispersion. *Ultrason Sonochem*. 2018;45(March):133-149. doi:10.1016/j.ultsonch.2018.03.007

31. Tobergte DR, Curtis S. *Ultrasound Technologies for Food Bioprocessing*. Vol 53.; 2013.

32. Hassan M, Reddy KR, Haque E, Minett AI, Gomes VG. High-yield aqueous phase exfoliation of graphene for facile nanocomposite synthesis via emulsion polymerization. *J Colloid Interface Sci*. 2013;410:43-51. doi:10.1016/j.jcis.2013.08.006

33. Strano MS, Moore VC, Miller MK, et al. The role of surfactant adsorption during ultrasonication in the dispersion of single-walled carbon nanotubes. *J Nanosci Nanotechnol*. 2003;3(1-2):81-86. doi:10.1166/jnn.2003.194

34. Lebon GSB, Tzanakis I, Pericleous K, Eskin D, Grant PS. Ultrasonic liquid metal processing:

The essential role of cavitation bubbles in controlling acoustic streaming. *Ultrason Sonochem*. 2019;55(September 2018):243-255. doi:10.1016/j.ultsonch.2019.01.021

35. Rubinetti D, Weiss DA, Wahlen A, Müller J. Numerical Modeling and Validation Concept for Acoustic Streaming Induced by Ultrasonic Treatment. *2016 COMSOL Conf Munich*. Published online 2016:12-14. https://www.comsol.com/paper/download/357161/rubinetti_paper.pdf%0Ahttps://www.comsol.com/paper/numerical-modeling-and-verification-of-acoustic-streaming-induced-by-ultrasonic--38061

36. Rubinetti D, Weiss DA. Ultrasound-driven fluid motion - Modelling approach. *Int J Multiphys*. 2018;12(1):1-8. doi:10.21152/1750-9548.12.1.1

37. Xu Z, Yasuda K, Koda S. Numerical simulation of liquid velocity distribution in a sonochemical reactor. *Ultrason Sonochem*. 2013;20(1):452-459. doi:10.1016/j.ultsonch.2012.04.011

38. Lebon B, Tzanakis I, Pericleous K, Eskin D. Numerical modelling of the ultrasonic treatment of aluminium melts: An overview of recent advances. *Materials (Basel)*. 2019;12(19). doi:10.3390/ma12193262

39. Trujillo FJ, Knoerzer K. A computational modeling approach of the jet-like acoustic streaming and heat generation induced by low frequency high power ultrasonic horn reactors. *Ultrason Sonochem*. 2011;18(6):1263-1273. doi:10.1016/j.ultsonch.2011.04.004

40. Moriyama T, Yoshizawa S, Umemura SI. Thermal simulation of cavitation-enhanced ultrasonic heating verified with tissue-mimicking gel. *Jpn J Appl Phys*. 2012;51(7 PART2). doi:10.1143/JJAP.51.07GF27

41. Solovchuk MA, Sheu TWH, Lin WL, Kuo I, Thiriet M. Simulation study on acoustic streaming and convective cooling in blood vessels during a high-intensity focused ultrasound thermal ablation. *Int J Heat Mass Transf*. 2012;55(4):1261-1270. doi:10.1016/j.ijheatmasstransfer.2011.09.023

42. Trujillo FJ, Knoerzer K. A computational modeling approach of the jet-like acoustic streaming and heat generation induced by low frequency high power ultrasonic horn reactors. *Ultrason Sonochem*. 2011;18(6):1263-1273. doi:10.1016/j.ultsonch.2011.04.004

43. Chemat F, Rombaut N, Sicaire AG, Meullemiestre A, Fabiano-Tixier AS, Abert-Vian M. Ultrasound assisted extraction of food and natural products. Mechanisms, techniques, combinations, protocols and applications. A review. *Ultrason Sonochem*. 2017;34:540-560. doi:10.1016/j.ultsonch.2016.06.035

44. Louisnard O. A simple model of ultrasound propagation in a cavitating liquid. Part I: Theory, nonlinear attenuation and traveling wave generation. *Ultrason Sonochem*. 2012;19(1):66-76. doi:10.1016/j.ultsonch.2011.06.008

45. Huang J, Holt RG, Cleveland RO, Roy RA. Experimental validation of a tractable numerical model for focused ultrasound heating in flow-through tissue phantoms. *J Acoust Soc Am*. 2004;116(4):2451-2458. doi:10.1121/1.1787124

46. Pasumarthi P. Investigation of Geometric Effect on the Ultrasonic Processing of Liquids. *TigerPrints*. Published online 2016. https://tigerprints.clemson.edu/all_theses/2447%0Ahttps://tigerprints.clemson.edu/all_theses/2447%0Ahttp://tigerprints.clemson.edu/all_theses/2447

47. Dopp JL, Jo YR, Reuel NF. Methods to reduce variability in E. Coli-based cell-free protein

expression experiments. *Synth Syst Biotechnol*. 2019;4(4):204-211.

doi:10.1016/j.synbio.2019.10.003